Tokyo Climate Center, Japan Meteorological Agency

TCC News

No. 40 Spring 2015

Contents

JMA's New Seasonal Ensemble Prediction System (JMA/MRI-CPS2)

A new version of JMA's Seasonal Ensemble Prediction System (JMA/MRI-CPS2) is scheduled to replace the current operational system (JMA/MRI-CPS1) in June 2015. The Seasonal Ensemble Prediction System (EPS) is used to produce three-month and warm/cold season predictions as well as for El Niño monitoring and outlook work. Changes in the new version include improved resolution and physics in the model's atmospheric and oceanic components and the introduction of an interactive sea ice model. In the new real-time operational suite, 51-member ensemble integrations are carried out from consecutive initial dates with intervals of five days. This is the same as the configuration of JMA/MRI-CPS1, except for an increase in the number of ensembles per initial date from 9 to 13 (Figure 1). Verification of re-forecasts (hindcasts) shows that JMA/MRI-CPS2 has higher predictive skill than JMA/MRI-CPS1 for three-month, warm/cold season and El Niño predictions.

Binary data currently distributed in GRIB-2 format will be modified in relation to the aforementioned ensemble members and composed initial dates. To support user calibration at NMHSs, the full set of re-forecasts is now available on the TCC website. It should be noted that some re-forecast initial dates differ from those of JMA/MRI-CPS1.

1. Outlines of the new system

The new seasonal EPS has the same atmosphere-ocean coupled general circulation model (CGCM) as the current one, but with the addition of interactive sea ice coupling. The new CGCM (JMA/MRI-CGCM2) has been upgraded with higher resolution in its atmospheric and oceanic components. The atmospheric model has a resolution of TL159 (approx. 110 km grid spacing) with 60 levels (0.1 hPa at the top), and the meridional resolution of the oceanic model has been increased from 1 to a maximum of 0.5 deg. The ocean model domain has been expanded to the global ocean via the use of a tripolar grid.

The model's physics have been improved in a variety of areas, including cumulus convection, cloud, radiation, sea-surface boundary in the atmosphere, and the ocean mixed layer and radiation in the ocean. Furthermore realistic concentration of greenhouse gases (GHGs) is prescribed in model integrations based on the CMIP5 RCP4.5 scenario, and land conditions are initialized using JRA-55 reanalysis data (Kobayashi et al. 2015). Atmospheric initial conditions are also taken from the JRA-55 analysis, and oceanic initial conditions are given from an improved version of an ocean assimilation system (MOVE/MRI.COM-G2).

The lagged average forecasting (LAF) approach is adopted to produce ensemble initial conditions along with a breeding of growing mode (BGM) method, which is similar to the technique used for JMA/MRI-CPS1. A stochastic physics scheme has also been introduced to better represent model uncertainty.

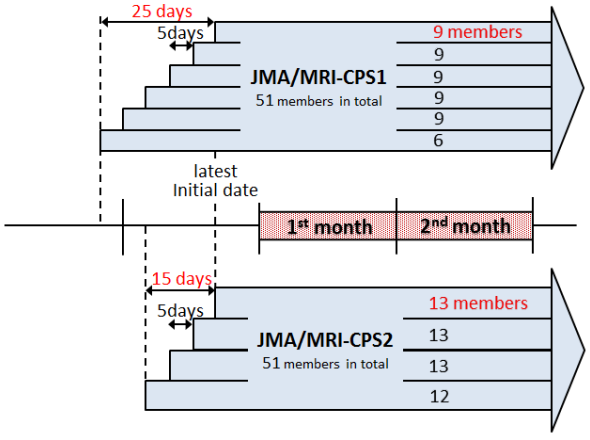

Figure 1 Schematic figure of ensemble configurations in the JMA/MRI-CPS1 and JMA/MRI-CPS2

Ensemble configurations of the operational suite are schematically illustrated in Figure 1. Thirteen-member ensemble integrations are made from consecutive initial dates with five-day intervals. In the new system, the number of ensembles per initial date has been increased from 9 to 13. This enables the production of combined 51-member ensemble predictions starting from later initial dates compared to the current system (Figure 1). As such, the forecast lead time is shortened.

2. Prediction performance

ENSO predictive skill is illustrated in Figure 2 with anomaly correlation coefficients (ACCs) of NINO3 (150 – 90°W, 5°S – 5°N) SSTs between COBE-SST analysis and predictions. Scores are computed with 10-member ensemble predictions starting every month for the period from 1981 to 2010. ENSO predictive skill is improved overall for all lead times, with remarkable improvement in scores for predictions beyond spring (i.e., the spring predictive barrier) (not shown).

Figure 3 shows ACCs averaged over the Northern Hemisphere (20 – 90°N) for three-month average 2-m temperature between the JRA-55 reanalysis and predictions. Figure 4 shows ACCs averaged over the tropics (20°S – 20°N) for three-month average precipitation between the GPCP version 2.2 analysis and predictions. JMA/MRI-CPS2 exhibits enhanced performance over JMA/MRI-CPS1 in 2-m temperature and precipitation predictions from all initial months. Scores for other elements are also improved overall. More detailed verification information is provided on the TCC website.

(Yuhei Takaya, Climate Prediction Division)

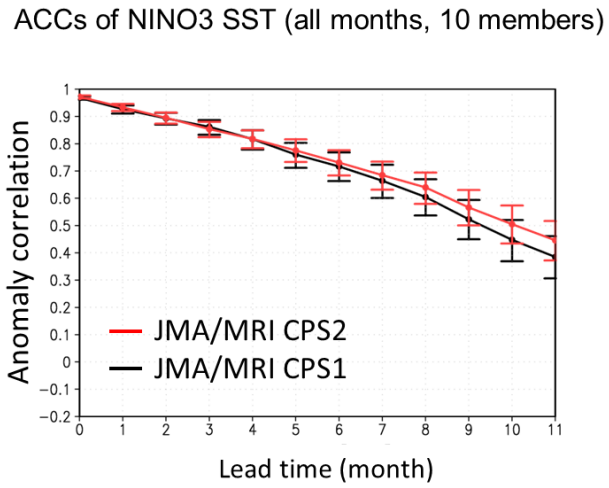

Figure 2 ACCs between observed and predicted NINO3 SST with respect to forecast lead time.
The red and black lines indicate ACCs of JMA/MRI-CPS2 and JMA/MRI-CPS1, respectively.

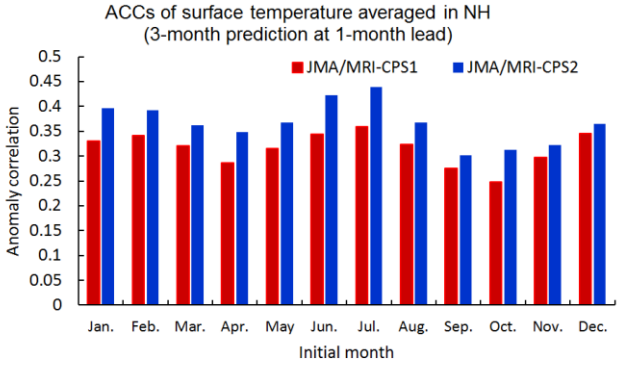

Figure 3 Northern Hemisphere average of ACCs between observed and predicted three-month averaged 2-m temperature with respect to initial months.
The blue and red bars indicate ACCs of JMA/MRI-CPS2 and JMA/MRI-CPS1, respectively.

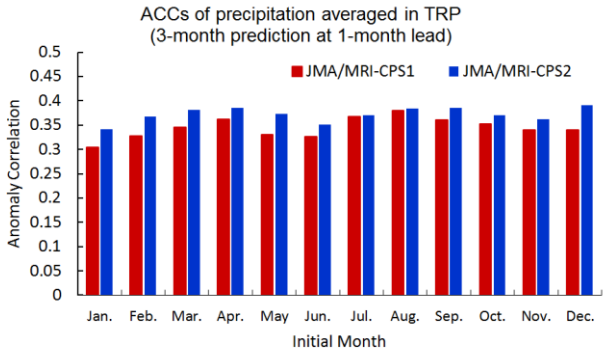

Figure 4 Tropics average of ACCs between observed and predicted three-month averaged precipitation with respect to initial months.
The blue and red bars indicate ACCs of JMA/MRI-CPS2 and JMA/MRI-CPS1, respectively.

El Niño Outlook (April – October 2015)

It is likely that El Niño conditions will redevelop by boreal summer 2015. ***(This article was written based on El Nino outlook issued on 10 April 2015.)***

El Niño/La Niña

In March 2015, the NINO.3 SST was near normal with a deviation of +0.2°C. SSTs (Figures 5 and 7 (a)) were remarkably above normal in the central equatorial Pacific. Subsurface temperatures (Figures 6 and 7 (b)) were above normal in the central equatorial Pacific. Atmospheric convective activity was significantly above normal near the date line over the equatorial Pacific, while easterly winds in the lower troposphere were near normal in the central Pacific. These oceanic and atmospheric conditions indicate that the El Niño event, which emerged in boreal summer 2014, probably ended in winter 2015 and that ENSO-neutral conditions currently prevail.

The subsurface warm waters of the central equatorial Pacific are expected to migrate eastward and to maintain warmer-than-normal SST conditions in the eastern part. According to JMA's El Niño prediction model, the NINO.3 SST will be above normal in the months ahead (Figure 8). In conclusion, El Niño conditions are likely to redevelop by boreal summer 2015.

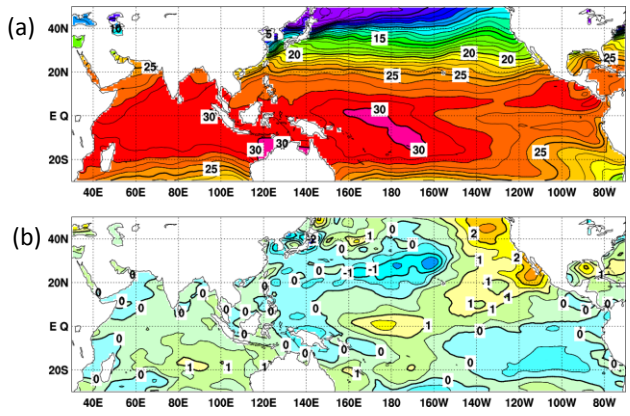

Figure 5 Monthly mean (a) sea surface temperatures (SSTs) and (b) SST anomalies in the Indian and Pacific Ocean areas for March 2015

The contour intervals are 1˚C in (a) and 0.5˚C in (b). The base period for the normal is 1981 – 2010.

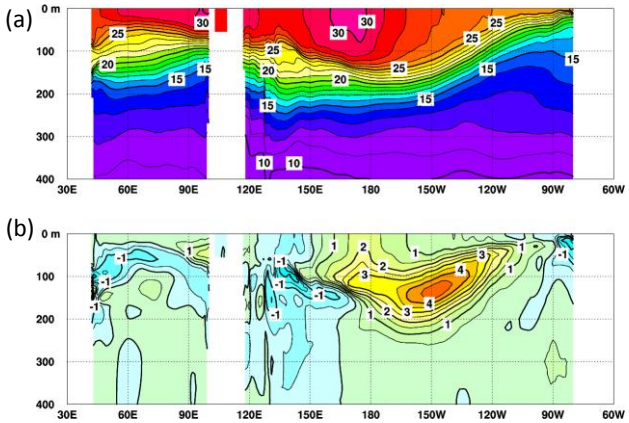

Figure 6 Monthly mean depth-longitude cross sections of (a) temperatures and (b) temperature anomalies in the equatorial Indian and Pacific Ocean areas for March 2015

The contour intervals are 1˚C in (a) and 0.5˚C in (b). The base period for the normal is 1981 – 2010.

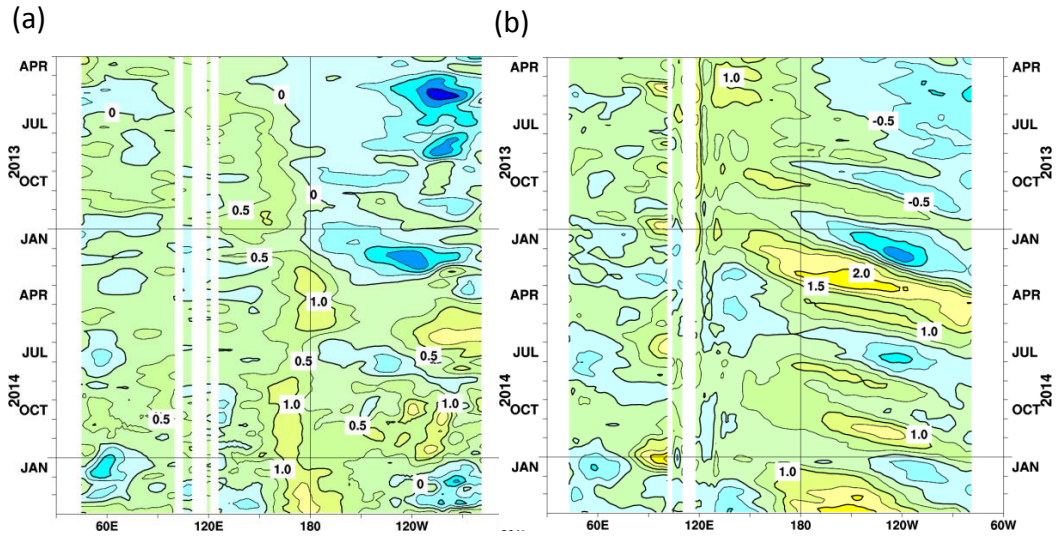

Figure 7 Time-longitude cross sections of (a) SST and (b) ocean heat content (OHC) anomalies along the equator in the Indian and Pacific Ocean areas

OHCs are defined here as vertical averaged temperatures in the top 300 m. The base period for the normal is 1981 – 2010.

Western Pacific and Indian Ocean

The area-averaged SST in the tropical western Pacific (NINO.WEST) region was below normal in March, and is likely to be near normal or below normal until boreal summer.

The area-averaged SST in the tropical Indian Ocean (IOBW) region was near normal in March, and is likely to be mostly near normal until boreal summer.

(Ikuo Yoshikawa, Climate Prediction Division)

* The SST normal for NINO.3 region (5°S – 5°N, 150°W – 90°W) is defined as an monthly average over a sliding 30-year period (1985-2014 for this year).
* The SST normals for the NINO.WEST region (Eq. – 15°N, 130°E – 150°E) and the IOBW region (20°S – 20°N, 40°E – 100°E) are defined as linear extrapolations with respect to a sliding 30-year period, in order to remove the effects of significant long-term warming trends observed in these regions.

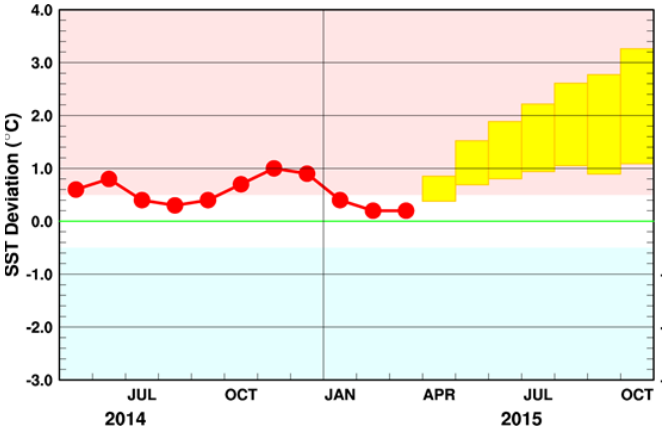

Figure 8 Outlook of NINO.3 SST deviation produced by the El Niño prediction model

This figure shows a time series of monthly NINO.3 SST deviations. The thick line with closed circles shows observed SST deviations, and the boxes show the values produced for the next six months by the El Niño prediction model. Each box denotes the range into which the SST deviation is expected to fall with a probability of 70%.

JMA's Seasonal Numerical Ensemble Prediction for Boreal Summer 2015

Based on JMA's seasonal ensemble prediction system, sea surface temperature (SST) anomalies in the equatorial Pacific Ocean are predicted to be above normal this boreal summer, suggesting a likely redevelopment of El Niño conditions. In association with the expected El Niño conditions, active convection is predicted over the eastern Pacific. Conversely, inactive convection is predicted over the Maritime Continent and the Indian Ocean. In line with this prediction, southward shifting of the subtropical jet stream is expected over Eurasia. The North Pacific High is also expected to be weaker than normal over most parts of the North Pacific except in the area southeast of Japan.

1. Introduction

This article outlines JMA's dynamical seasonal ensemble prediction for boreal summer 2015 (June – August, referred to as JJA), which was used as a basis for the Agency's operational warm-season outlook issued on 24 April 2015. The outlook detailed here is based on the seasonal ensemble prediction system of the Coupled atmosphere-ocean General Circulation Model (CGCM). See the column below for system details.

Section 2 outlines global SST anomaly predictions, and Section 3 describes the associated circulation fields expected over the tropics and sub-tropics. Finally, the circulation fields predicted for the mid- and high- latitudes of the Northern Hemisphere are discussed in Section 4.

2. SST anomalies (Figure 9)

Figure 9 shows predicted SSTs (contours) and related anomalies (shading) for JJA. SST anomalies in the equatorial Pacific Ocean are predicted to be above normal throughout the period, suggesting a likely redevelopment of El Niño conditions. They are also predicted to be slightly above normal in the Indian Ocean. Conversely, SST anomalies are predicted to be slightly below normal in the Philippine Sea.

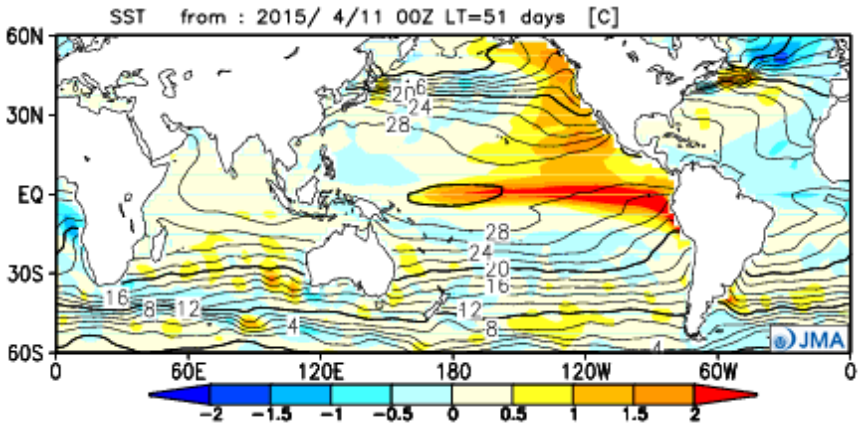

Figure 9
Predicted SSTs (contours) and SST anomalies (shading) for June–August 2015 (ensemble mean of 51 members)

3. Prediction for the tropics and sub-tropics (Figure 10)

Figure 10 (a) shows predicted precipitations (contours) and related anomalies (shading) for JJA. In association with the expected El Niño condition, precipitation anomalies over the equatorial Pacific Ocean are predicted to be above normal. Those over the Philippine Sea are also predicted to be slightly above normal despite slightly below normal SSTs. However this should be interpreted with caution, due to dependence on unpredictable tropical cyclone activity. Conversely, those over the Maritime Continent and the equatorial Atlantic Ocean are predicted to be below normal. Those over most of South Asia are also predicted to be slightly below normal.

Figure 10 (b) shows predicted velocity potentials (contours) and related anomalies (shading) for JJA at the upper troposphere (200hPa). Velocity potential anomalies at 200hPa are predicted to be negative (i.e., divergent) over the eastern Pacific, reflecting active convection over the equatorial Pacific Ocean. Conversely, positive (i.e., convergent) anomalies are predicted over the Maritime Continent and the Indian Ocean, reflecting inactive convection in and around these regions.

Figure 10 (c) shows predicted stream functions (contours) and related anomalies (shading) for JJA at the upper troposphere (200hPa). In association with inactive convection over the Maritime Continent and the Indian Ocean, stream function anomalies at 200hPa are predicted to be negative (i.e., cyclonic) over Eurasia, indicating a southward-shifting tendency for the subtropical jet stream. Conversely, positive (i.e., anti-cyclonic) anomalies are predicted over the North Pacific as a response from above-normal precipitation over the equatorial Pacific Ocean.

Figure 10 (d) shows predicted stream functions (contours) and related anomalies (shading) for JJA at the lower troposphere (850hPa). Stream function anomalies at 850hPa are predicted to be negative (i.e., cyclonic) over the North Pacific, suggesting a weak Pacific High.

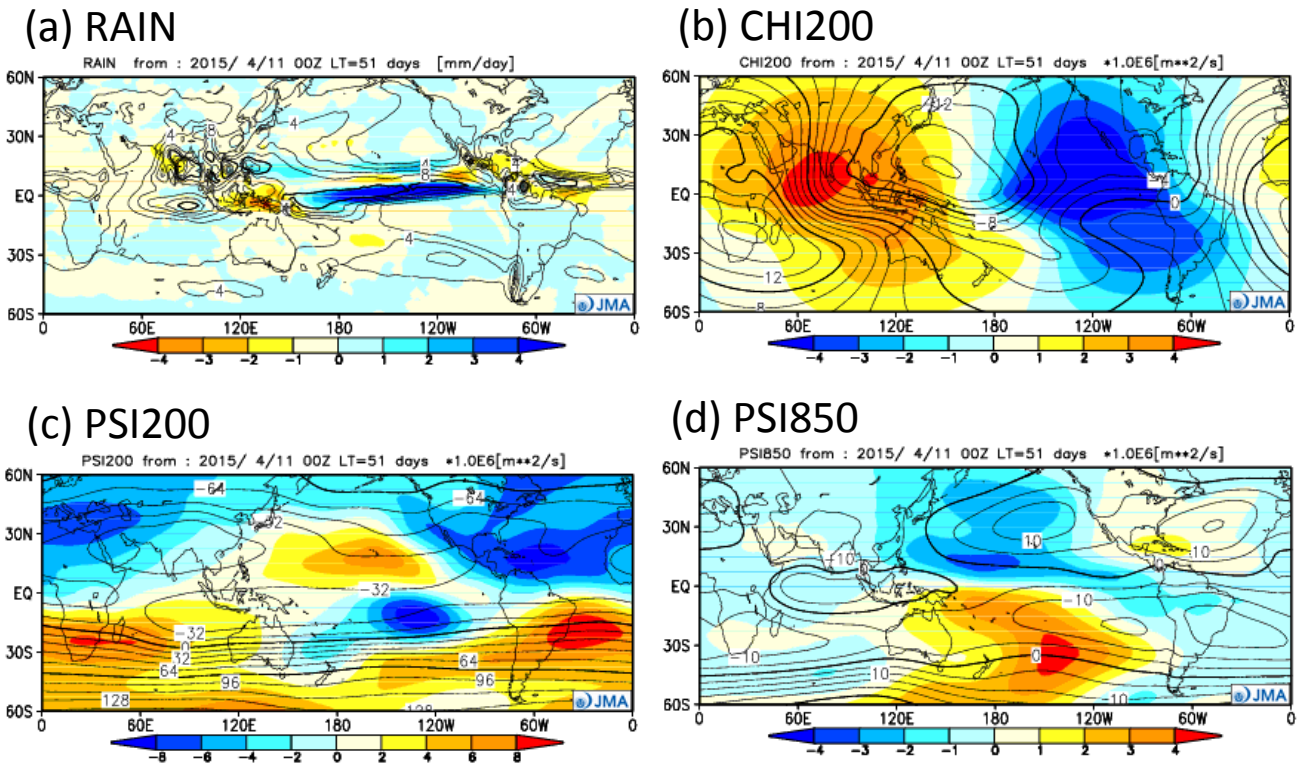

Figure 10 Predicted atmospheric fields from 60°N – 60°S for June–August 2015 (ensemble mean of 51 members)

(a) Precipitation (contours) and anomaly (shading). The contour interval is 2 mm/day.

(b) Velocity potential at 200 hPa (contours) and anomaly (shading). The contour interval is 2×10^6 m^2/s.

(c) Stream function at 200 hPa (contours) and anomaly (shading). The contour interval is 16×10^6 m^2/s.

(d) Stream function at 850 hPa (contours) and anomaly (shading). The contour interval is 5×10^6 m^2/s.

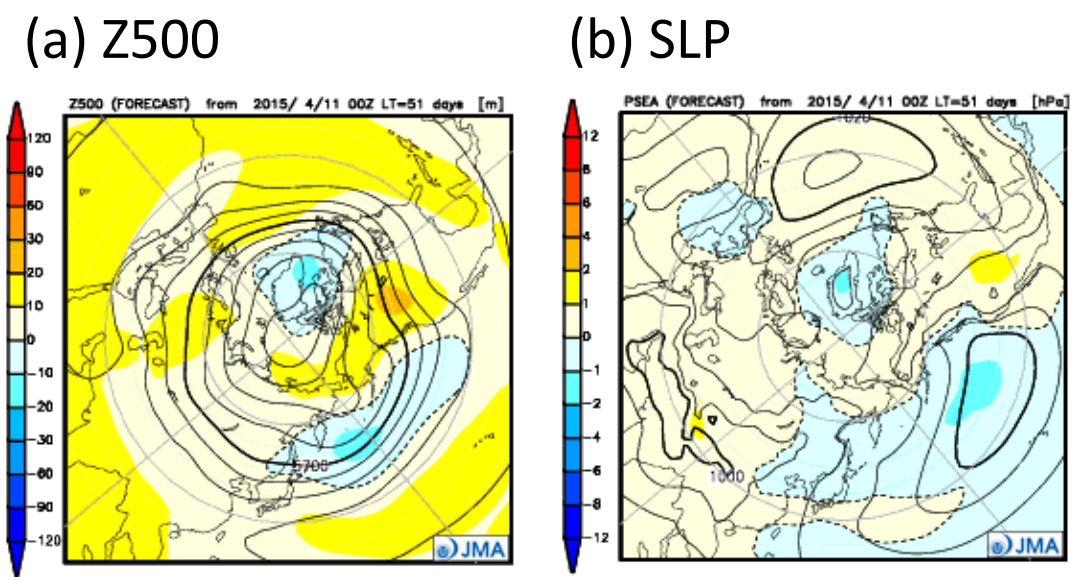

Figure 11 Predicted atmospheric fields from 60°N – 60°S for June–August 2015 (ensemble mean of 51 members)
(a) Geopotential height at 500hPa (contours) and anomaly (shading). The contour interval is 60 m.
(b) Sea level pressure (contours) and anomaly (shading). The contour interval is 4hPa.

4. Prediction for the mid- and high- latitudes of the Northern Hemisphere (Figure 11)

Figure 11 (a) shows predicted geopotential heights (contours) and related anomalies (shading) for JJA at 500hPa. Geopotential height anomalies at 500hPa are predicted to be positive over most of Northern Hemisphere, reflecting a global warming trend. However, negative anomalies are predicted over the northern part of the North Pacific and Greenland in association with a wave train propagating from the equatorial Pacific to the northern part of North America.

Figure 11 (b) shows predicted sea level pressures (contours) and related anomalies (shading) for JJA. Sea level pressure anomalies are predicted to be negative over the most part of North Pacific except in the area southeast of Japan, suggesting a diminished North Pacific High.

(Takashi Yamada, Climate Prediction Division)

JMA's Seasonal Ensemble Prediction System

JMA operates a seasonal Ensemble Prediction System (EPS) using the Coupled atmosphere-ocean General Circulation Model (CGCM) to make seasonal predictions beyond a one-month time range. The EPS produces perturbed initial conditions by means of a combination of the initial perturbation method and the lagged average forecasting (LAF) method. The prediction is made using 51 members from the latest six initial dates (nine members are run every five days). Details of the prediction system and verification maps based on 30-year hindcast experiments (1981–2010) are available at http://ds.data.jma.go.jp/tcc/tcc/products/model/.

Warm Season Outlook for Summer 2015 in Japan

In summer 2015, mean temperatures are expected to be either near or above normal (both with 40% probability) in eastern Japan. Warm-season precipitation amounts are expected to be near or above normal (both with 40% probability) in northern Japan.

1. Outlook summary (Figure 12)

JMA issued its outlook for the coming summer (June – August) 2015 over Japan in February and updated it in March and April based on the Agency's seasonal Ensemble Prediction System (EPS). This article outlines the outlook update of 25 March.

Mean temperatures in summer are expected to be near or above normal, both with 40% probability, in eastern Japan, and to be within a near-normal range in other parts of the country. Warm-season precipitation amounts are expected to be near or above normal, both with 40% probability, in northern Japan, and to be within a near-normal range in other parts of the country. Rainy season (Baiu) precipitation amounts are unlikely to exhibit particular characteristics in any region.

2. Outlook background

Figure 13 shows a conceptual diagram highlighting expected large-scale ocean/atmosphere characteristics for summer. An outline of the background to the outlook is given below.

- Sea surface temperatures (SSTs) are expected to be above normal over the equatorial Pacific. According to the El Niño Outlook issued on 10 March, there is a higher likelihood of a redevelopment of El Niño conditions in the Northern Hemisphere summer than of continued ENSO-neutral conditions.
- Convection over the tropics is expected to be more active than normal over the equatorial Pacific and less active than normal from the northern Indian Ocean to the Maritime continent.
- The Tibetan High is expected to be weaker than normal in association with inactive convection from the northern Indian Ocean to the Maritime continent.
- The subtropical jet stream, which flows along the northern edge of the Tibetan High, is expected to shift southward of its normal position and to be stronger than normal around and east of Japan. This tendency would favor enhancement of the frontal zone associated with the jet stream.
- The north Pacific High is expected to be weaker than normal in the northern part and near normal in southeast of Japan.
- Considering the above, a tendency for wetness is expected in northern Japan. In other parts of the country (except the Pacific side its eastern part), a slight tendency toward wetness within the normal range is expected.
- Overall temperatures in the troposphere are expected to be higher than normal, particularly in the lower latitudes of the westerlies, reflecting the recent warming tendency and high SSTs in the equatorial Pacific. This would support a warm tendency over Japan despite the wet and cool tendencies associated with the enhanced frontal zone.

(Masayuki Hirai, Climate Prediction Division)

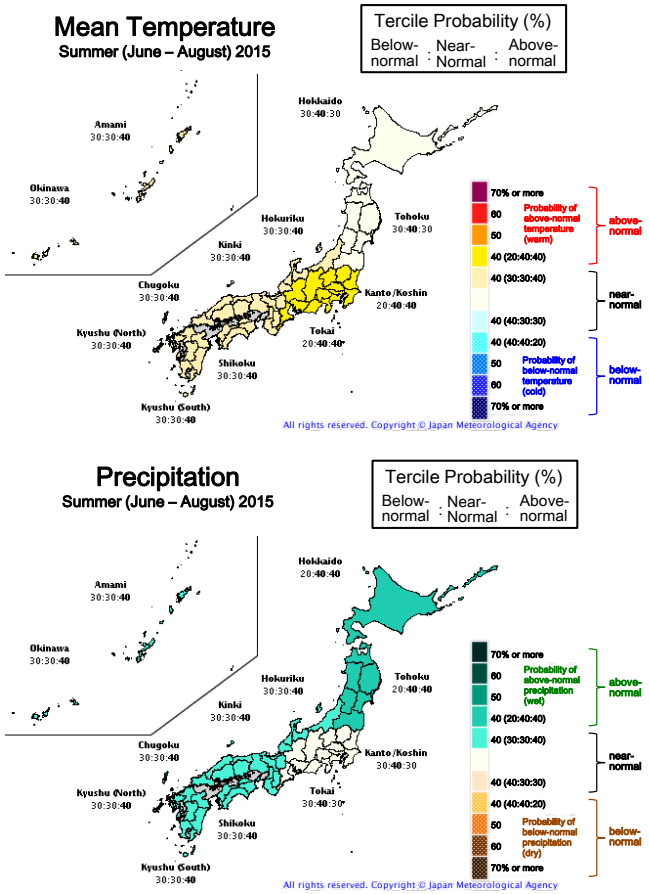

Figure 12 Outlook for summer 2015 temperature (above) and precipitation (below) probability in Japan.

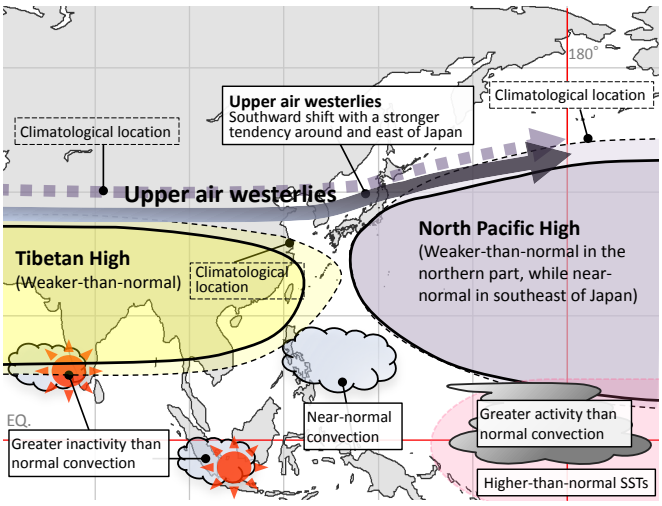

Figure 13 Schematic diagram showing expected large scale characteristics of ocean and atmosphere in summer 2015

Summary of the 2014/2015 Asian Winter Monsoon

This report summarizes the characteristics of the surface climate and atmospheric/oceanographic considerations related to the Asian winter monsoon for 2014/2015.

Note: The Japanese 55-year Reanalysis (JRA-55; Kobayashi et al. 2015) atmospheric circulation data and COBE-SST (JMA 2006) sea surface temperature (SST) data were used for this investigation. The outgoing longwave radiation (OLR) data referenced to infer tropical convective activity were originally provided by NOAA. The base period for the normal is 1981 – 2010. The term "anomaly" as used in this report refers to deviation from the normal.

1. Surface climate conditions

1.1 Overview of Asia

In boreal winter 2014/2015, temperatures were above or near normal in many parts of East Asia and in Siberia, and were below normal from seas south of Japan to the Philippines and around eastern India. Very low temperatures were recorded around Japan in December, and very high temperatures were recorded from Central Siberia to eastern China in January (Figure 14 and 23).

Figure 15 shows extreme climate events occurring between December 2014 and February 2015. In December, extremely low temperatures were observed in northwestern China and from Pakistan to northwestern India. Extremely heavy precipitation amounts were observed around Japan and from central Indonesia to Sri Lanka. In January, extremely high temperatures were seen in the eastern part of Eastern Siberia and from the southern part of Central Siberia to eastern China. Extremely heavy precipitation amounts were observed around the Indochina Peninsula. In February, extremely high temperatures were observed around the southern part of Eastern Siberia, and extremely heavy precipitation amounts were observed around the southern part of Central Asia.

Figure 16 shows a time-series representation of daily temperatures at New Delhi in India and Incheon in Republic of Korea during winter 2014/2015. Daily mean temperatures were below normal on many days from mid-December to late January, and were above normal in early December and the second half of February at New Delhi. Daily mean temperatures were below normal on many days in December, and were above normal on many days in January and February at Incheon.

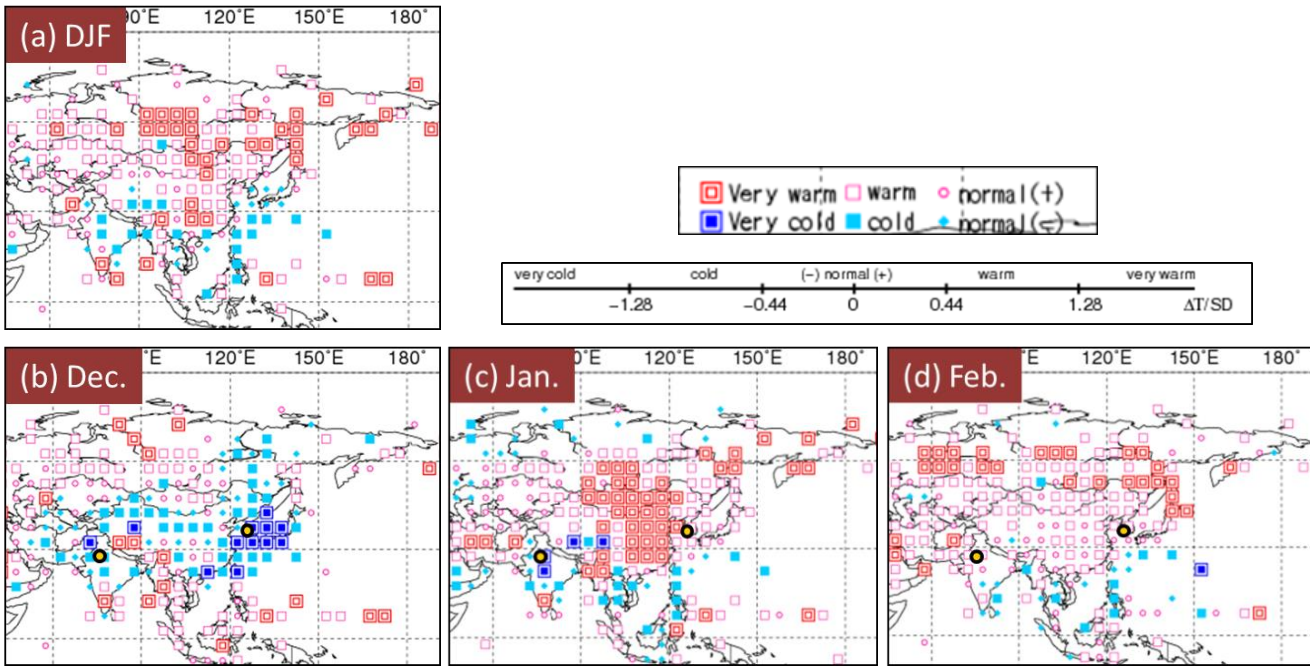

Figure 14 (a) Three-month mean temperature anomalies for December 2014 – February 2015, and monthly mean temperature anomalies for (b) December 2014, (c) January 2015 and (d) February 2015

Categories are defined by the three-month/monthly mean temperature anomaly against the normal divided by its standard deviation and averaged in 5° × 5° grid boxes. The thresholds of each category are -1.28, -0.44, 0, +0.44 and +1.28. Standard deviations were calculated from 1981 – 2010 statistics. Areas over land without graphical marks are those where observation data are insufficient or where normal data are unavailable. Orange-colored circles in figures (b) - (d) indicate locations of New Delhi (India) and Incheon (Republic of Korea). Daily temperature data for both cities are shown in Figure 16.

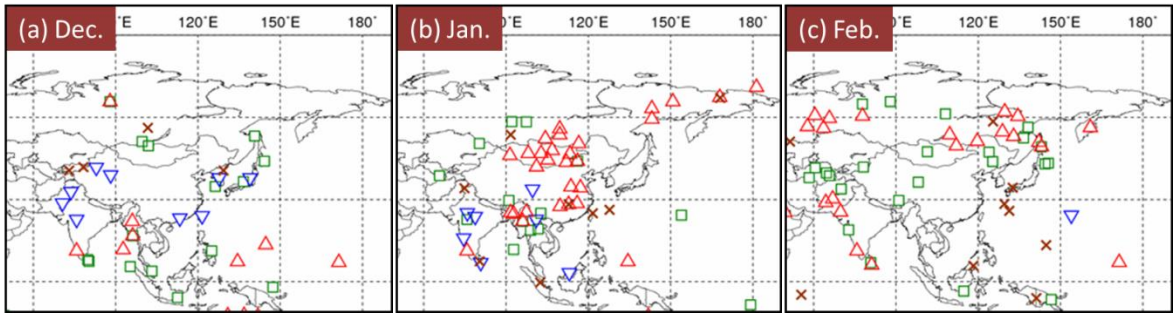

Figure 15 Extreme climate events for (a) December 2014, (b) January 2015 and (c) February 2015

△ Extremely high temperature (ΔT/SD > 1.83) □ Extremely heavy precipitation (Rd = 6)

▽ Extremely low temperature (ΔT/SD < -1.83) × Extremely light precipitation (Rd = 0)

ΔT, SD and Rd indicate temperature anomaly, standard deviation and quintile, respectively.

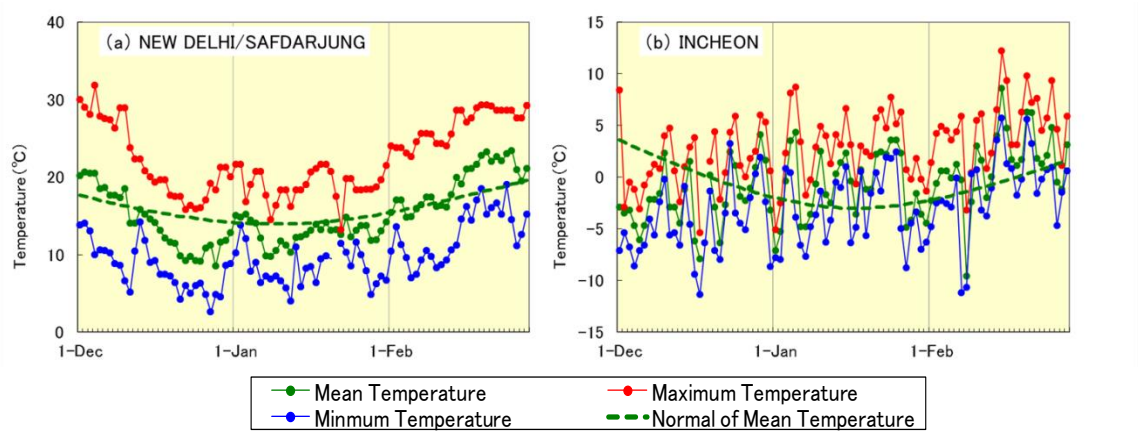

Figure 16 Time series of daily maximum, mean and minimum temperatures (°C) at New Delhi in India and Incheon in Republic of Korea from 1 December 2014 to 28 February 2015 (based on SYNOP reports)

2. Characteristic atmospheric circulation and oceanographic conditions

2.1 Conditions in the tropics and Asian Winter Monsoon

In winter 2014/2015, sea surface temperatures (SSTs) were above normal in the western-to-central equatorial Pacific and below normal in the western equatorial Indian Ocean (Figure 17). An active convection phase of the Madden-Julian Oscillation was seen propagating eastward from the Indian Ocean to the western Pacific from late November to early December, followed by another active phase from late December to early January, both with enhanced amplitude (Figure 18). Convective activity averaged over the three months from December to February was enhanced from the Maritime Continent to the western equatorial Pacific (Figure 19 (a)).

In December 2014, large-scale divergence anomalies in the upper troposphere were pronounced over the eastern equatorial Indian Ocean (Figure 19 (b)). These convection anomalies are thought to have served as a heating source in association with the development of a pattern with anticyclonic circulation anomalies centered over South China and cyclonic circulation anomalies seen around Japan (Figure 20 (b)), which contributed to enhanced cold air flow into East Asia. This is corroborated by a resemblance between the actual pattern of anticyclone-cyclone anomalies and the steady response seen in a linear baroclinic model (LBM) experiment forced with observed heating anomalies (Figure 21). It is therefore probable that the low temperatures experienced in East Asia during December were related to the enhanced convective activity observed over the eastern Indian Ocean.

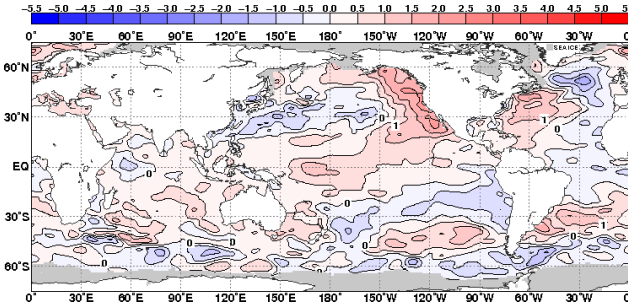

Figure 17 Three-month mean sea surface temperature (SST) anomalies for December 2014 – February 2015

The contour interval is 0.5°C.

In January 2015, anticyclonic circulation anomalies in the upper troposphere centered over East Asia (Figure 20 (c)) and the weaker-than-normal Siberian High (Figure 24 (c)) were related to the higher-than-normal temperatures recorded around eastern China (Figure 14 (c)). Upstream of these anticyclonic anomalies, cyclonic circulation anomalies were centered over the northern part of the Bay of Bengal, presumably in association with heavy precipitation experienced over parts of the Indochina Peninsula (Figure

15 (b)). These anomalies constituted a wave train pattern propagating eastward from the Middle East along the subtropical jet stream.

In February 2015, the subtropical jet stream over the area from South Asia to East Asia shifted southward of its normal position as indicated in Figure 20 (d) in association with suppressed convective activity around Indonesia.

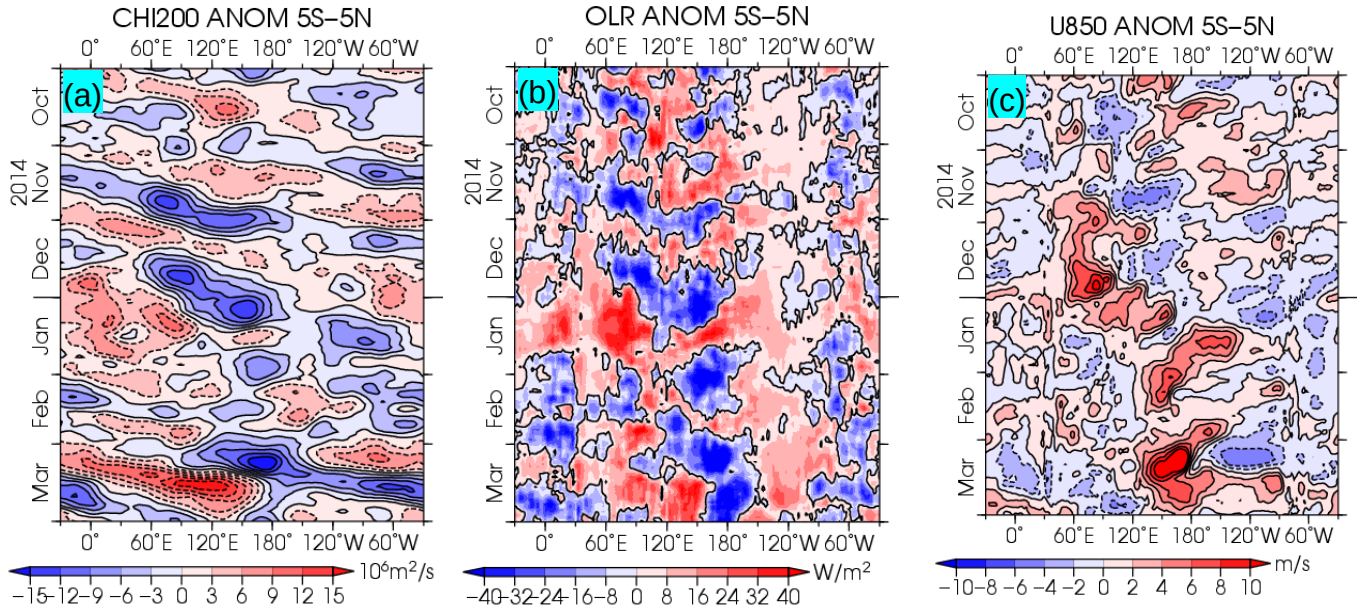

Figure 18 Time-longitude cross section of seven-day running mean (a) 200-hPa velocity potential anomalies, (b) outgoing longwave radiation (OLR) anomalies, and (c) 850-hPa zonal wind anomalies around the equator (5°S – 5°N) from October 2014 to March 2015

(a) The blue and red shading indicate areas of divergence and convergence anomalies, respectively. (b) The blue and red shading indicate areas of enhanced and suppressed convective activity, respectively. (c) The blue and red shading show easterly and westerly wind anomalies, respectively.

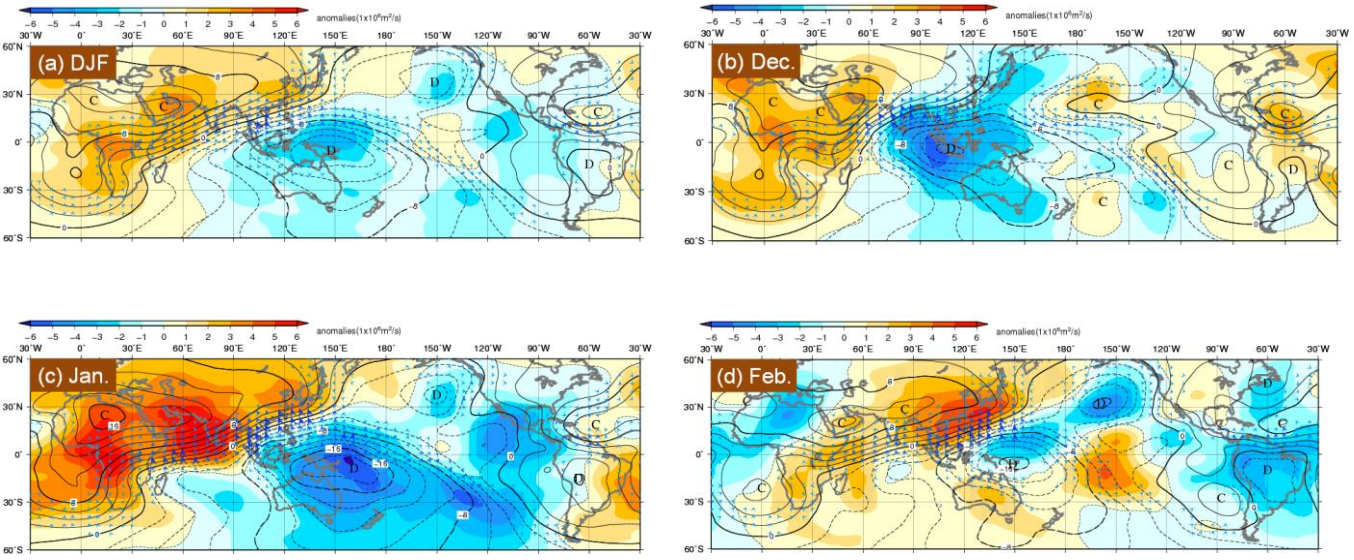

Figure 19 200-hPa velocity potential (a) averaged over the three months from December 2014 to February 2015, for (b) December 2014, (c) January 2015 and (d) February 2015

The contours indicate velocity potential at intervals of 2×10^6 m^2/s, and the shading shows velocity potential anomalies. D and C indicates the bottom and peak of velocity potential, corresponding to the centers of large-scale divergence and convergence, respectively.

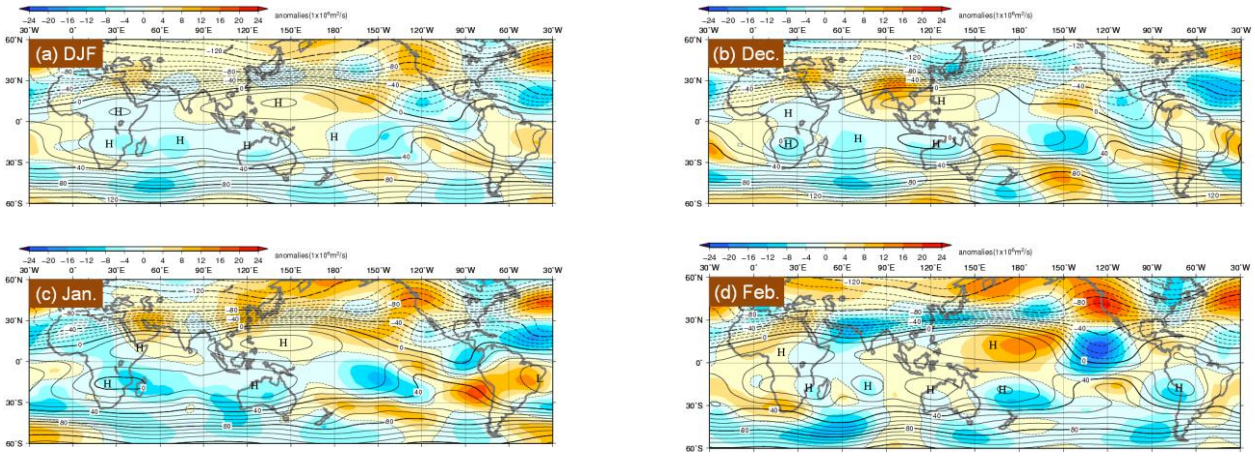

Figure 20 200-hPa stream function (a) averaged over the three months from December 2014 to February 2015, for (b) December 2014, (c) January 2015, and (d) February 2015

The contours indicate stream function at intervals of 10×10^6 m^2/s and the shadings indicate anomalies. H and L denote the centers of anticyclonic and cyclonic circulation anomalies, respectively.

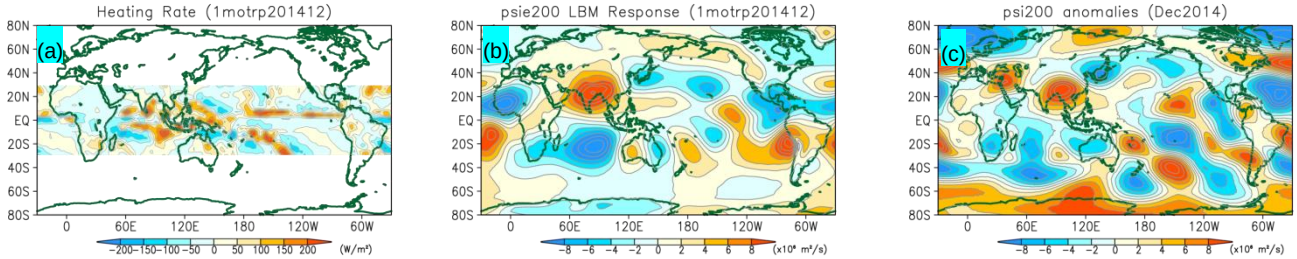

Figure 21 Steady response in a linear baroclinic model (LBM) to heating anomalies in the tropics for December 2014

(a) The red and blue shading indicates diabatic heating and cooling anomalies, respectively, for the LBM with the basic state for December (i.e., the 1981 – 2010 average). (b) The shading denotes the steady response of 200-hPa stream function anomalies (m^2/s). (c) The shading shows the actual 200-hPa stream function anomalies for December 2014. The anomalies in (b) represent deviations from the basic states, and are additionally subtracted from the zonal averages of the anomalies.

2.2 Conditions in the extratropics and Asian Winter Monsoon

In winter 2014/2015, the polar vortex tended to shift toward northeastern Canada in the 500-hPa height field (Figure 22 (a)). In association with distinct ridges persistent over the western part of North America (Figure 22 (a)), precipitation in the southwestern USA was below normal except in December, exacerbating the exceptionally dry conditions that have continued since 2013. As seen in the 500-hPa height field and the sea level pressure field, positive anomalies were persistent in the northern part of the North Atlantic throughout the winter (Figure 22 and 24) and repeatedly served as a source of wave activity propagating eastward through Europe towards East Asia. The intensity of the Siberian High varied throughout winter, being stronger than normal in the first half of December and from late January to early February and weaker than normal from late December to mid-January and in mid-February (Figure 25 (a)). Intensity averaged throughout the winter was close to normal (Figure 25 (b)).

In December 2014, a dipole-type blocking circulation developed over East Siberia (Figure 22 (b)). A wave-train pattern was noticeable along the polar front jet stream from the Atlantic Ocean eastward, indicating a contribution to negative height anomalies and low temperatures in East Asia.

In February 2015, an overall pattern with negative anomalies in the Arctic and positive anomalies in the mid-latitudes appeared in the 500-hPa height field in association with the positive phase of the Arctic Oscillation. Parts of the area from Eastern Siberia to northern Japan experienced extremely high temperatures, which were likely attributable to the weaker-than-normal Siberian High and a blocking-type ridge that developed around the Kamchatka Peninsula (Figure 22 (d)).

(Yoshinori Oikawa and Ayako Takeuchi, Tokyo Climate Center)

References

JMA, 2006: Characteristics of Global Sea Surface Temperature Data (COBE-SST), *Monthly Report on Climate System*, Separated Volume No. **12**.

Kobayashi, S., Y. Ota, Y. Harada, A. Ebita, M. Moriya, H. Onoda, K. Onogi, H. Kamahori, C. Kobayashi, H. Endo, K. Miyaoka, and K. Takahashi, 2015: The JRA-55 Reanalysis: General Specifications and Basic Characteristics. *J. Meteorol. Soc. Japan*, **93**, 5 – 48.

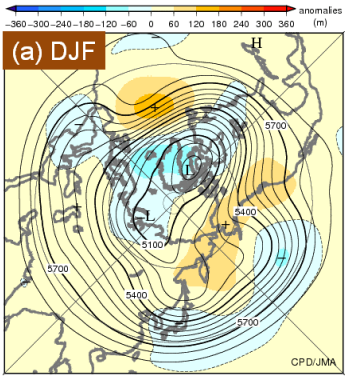

Figure 22 500-hPa height (a) averaged over the three months from December 2014 to February 2015, for (b) December 2014, (c) January 2015, and (d) February 2015

The contours indicate 500-hPa height at intervals of 60 m, and the shading denotes anomalies. H and L indicate the peak and bottom of 500-hPa height, respectively, and + (plus) and – (minus) show the peak and bottom of anomalies, respectively.

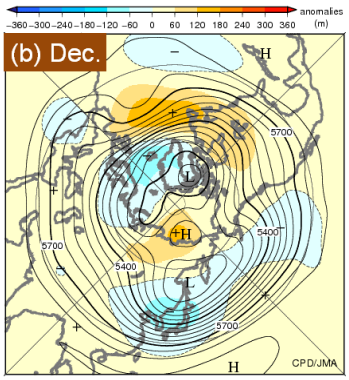

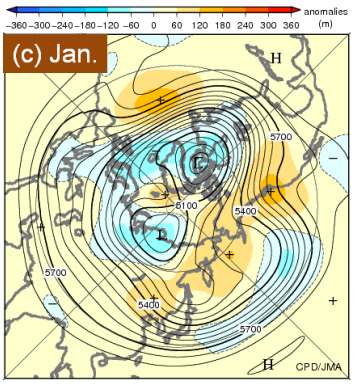

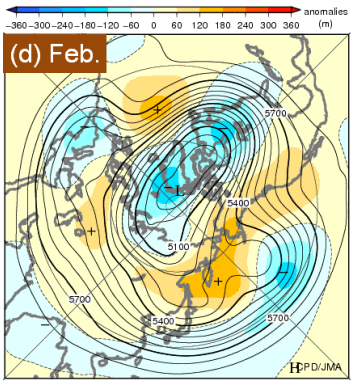

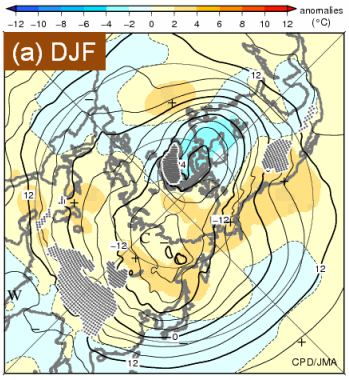

Figure 23 850-hPa temperature (a) averaged over the three months from December 2014 to February 2015, for (b) December 2014, (c) January 2015, and (d) February 2015

The contours indicate 850-hPa temperature at intervals of 4°C, and the shading denotes anomalies. W and C indicate the centers of warm and cold air, respectively, and + (plus) and – (minus) show the peak and bottom of 850hPa temperature anomalies, respectively.

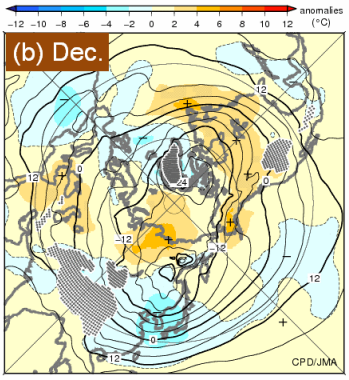

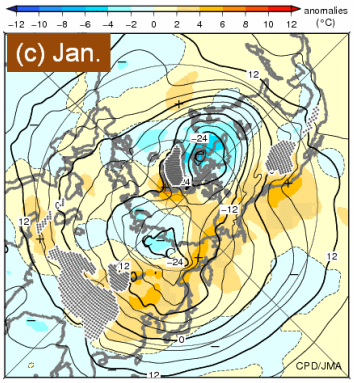

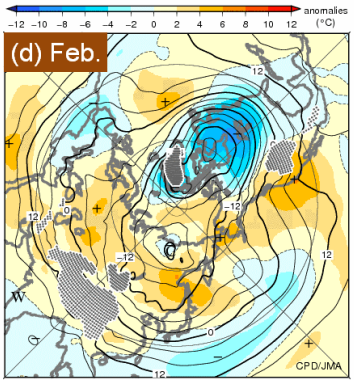

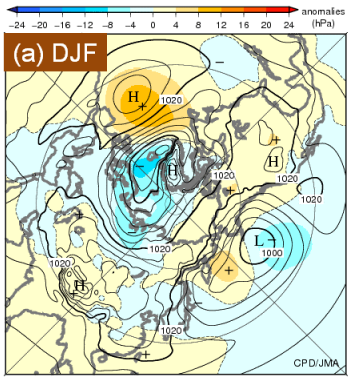

Figure 24 Sea level pressure (a) averaged over the three months from December 2014 to February 2015, for (b) December 2014, (c) January 2015 and (d) February 2015

The contours indicate sea level pressure at intervals of 4 hPa, and the shading shows related anomalies. H and L indicate the centers of high and low pressure systems, respectively, and + (plus) and – (minus) show the peak and bottom of sea level pressure anomalies, respectively.

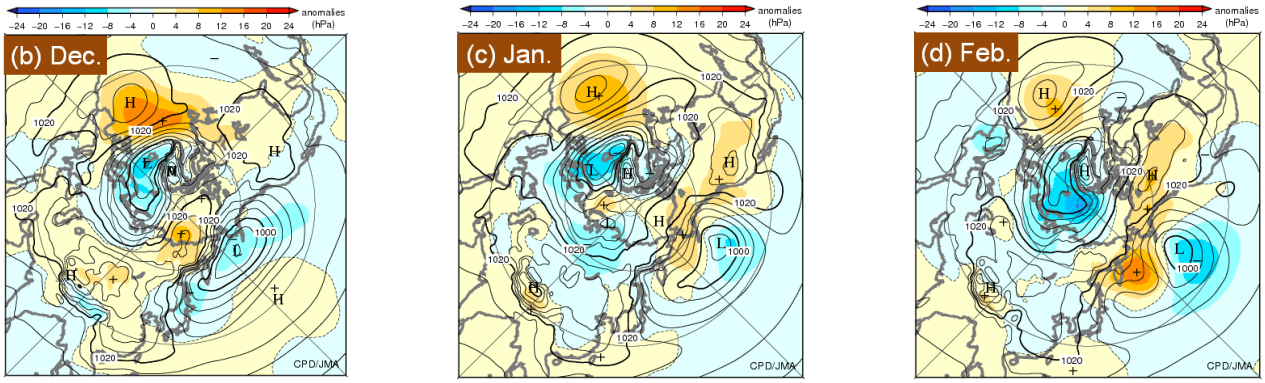

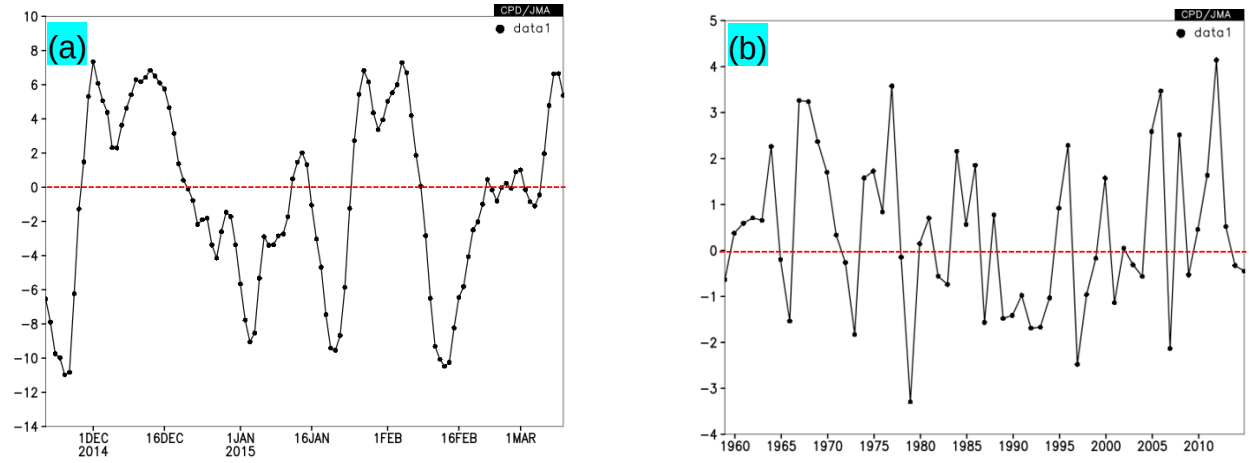

Figure 25 (a) Intraseasonal and (b) interannual variations of area-averaged sea level pressure anomalies around the center of the Siberian High (40°N – 60°N, 80°E – 120°E) for winter

(a) The black line indicates five-day running mean values from 21 November 2014 to 10 March 2015. (b) The black line indicates three-month mean values for winter from 1958/1959 to 2014/2015.

TCC Experts Visit Thailand

TCC arranges expert visits to NMHSs to support climate services and the effective transfer of technology. As part of such efforts, TCC experts visited the Thai Meteorological Department (TMD) in Thailand from 25 to 27 March 2015 to conduct follow-up activities regarding the generation of global warming prediction information covered at the TCC Training Seminar held in last January.

In the presence of around 12 TMD experts engaged in climate service provision, the visiting experts elucidated the generation of global warming prediction information using the latest 20-km-resolution global warming projection data produced by JMA's Meteorological Research Institute and gave an overview the basic guidance of iTacs (the Interactive Tool for Analysis of the Climate System). Using the same projection data, attendees then tried generating the global warming prediction information for Thailand for themselves. The visitors provided outstanding opportunities for attendees to learn more about global warming and discuss future collaboration with TCC.

TCC will continue to arrange expert visits to NMHSs in Southeast Asia and elsewhere as necessary to assist with operational climate services.

(Atsushi Goto, Tokyo Climate Center)

Any comments or inquiry on this newsletter and/or the TCC website would be much appreciated. Please e-mail to tcc@met.kishou.go.jp.

(Editors: Kazutoshi Onogi, Atsushi Goto and Yasushi Mochizuki)

Tokyo Climate Center (TCC), Japan Meteorological Agency
Address: 1-3-4 Otemachi, Chiyoda-ku, Tokyo 100-8122, Japan
TCC Website: http://ds.data.jma.go.jp/tcc/tcc/index.html